Comput Geosci
DOI 10.1007/s10596-009-9148-8

ORIGINAL PAPER

Deformation band populations in fault damage zone—impact on fluid flow

Dmitry Kolyukhin · Sylvie Schueller · Magne S. Espedal · Haakon Fossen

Received: 1 December 2008 / Accepted: 29 June 2009

Abstract Fault damage zones in highly porous reservoirs are dominated by deformation bands that generally have permeability-reducing properties. Due to an absence of sufficiently detailed measurements and the irregular distribution of deformation bands, a statistical approach is applied to study their influence on flow. A stochastic model of their distribution is constructed, and band density, distribution, orientation, and flow properties are chosen based on available field observations. The sensitivity of these different parameters on the upscaled flow is analyzed. The influence of a heterogeneous permeability distribution was also studied by assuming the presence of high permeability holes within bands. The fragmentation and position of these holes affect significantly the block-effective permeability. Results of local upscaling with a diagonal and full upscaled permeability tensor are compared, and qualitatively similar results for the flow characteristics are obtained. Further, the procedure of iterative local–global upscaling is applied to the problem.

D. Kolyukhin (✉) · S. Schueller · M. S. Espedal · H. Fossen
Centre for Integrated Petroleum Research,
University of Bergen, Allégaten 41, 5007 Bergen, Norway
e-mail: dmitriy.kolyukhin@cipr.uib.no

M. S. Espedal
e-mail: magne.espedal@cipr.uib.no

H. Fossen
e-mail: haakon.fossen@geo.uib.no

Present Address:
S. Schueller
IFP, 1&4 avenue de Bois-Préau,
92852 Rueil-Malmaison Cedex, France
e-mail: sylvie.schueller@ifp.fr

Keywords Fault damage zone · Deformation band · Effective permeability · Stochastic models · Upscaling

1 Introduction

In reservoirs, fault zones represent tabular zones of deformed rock that introduce significant petrophysical anisotropy, which potentially perturbs fluid flow during production. Fault zones are typically composed of a fault core, which accumulates most of the displacement, and an enveloping damage zone [33]. Even though the fault core represents the most heterogeneous structural element in a deformed reservoir rock, the damage zone can have an additional impact on fluid flow. The damage zone is a deformed rock volume that comprises various subsidiary tectonic elements, notably structural discontinuities such as minor faults and slip surfaces, veins, and features known as deformation bands and deformation band clusters.

Deformation bands are millimeter thick deformation zones, typically with shear offsets that rarely exceed a few centimeters even though their length can exceed 100 m (see [14] for a review). They occur in highly porous reservoirs (∼15% or higher porosity), particularly in fault damage zones, and are found not only as single structures but also as clusters, especially close to the fault core (Fig. 1). Their formation involves grain reorganization by grain sliding, rotation, and/or fracture, most commonly during compaction-assisted shearing. The internal changes in grain arrangement can modify the porosity and permeability within the band. This is particularly true for cataclastic deformation bands (Fig. 1), in which grain size is reduced by grain fracturing and permeability reductions of several

Published online: 10 July 2009

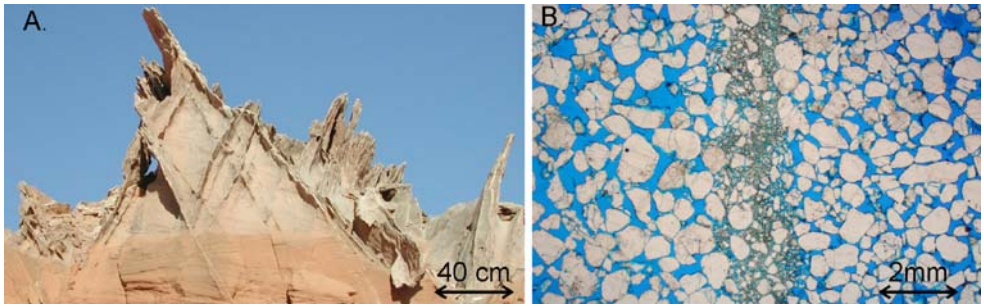

Fig. 1 **A** Deformations bands in the Entrada sandstone in Utah [13]. Note the distribution in clusters as well as the conjugate arrangement. **B** Photomicrograph of a single cataclastic deformation band displaying a reduction of porosity due to grain crushing

orders of magnitude is common (e.g., [13]). Cataclastic deformation bands in porous siliciclastic sedimentary rocks may, thus, potentially baffle fluid flow (e.g., [14]) at least at reservoir production timescale.

The small thicknesses of deformation bands make their real influence on fluid flow in reservoirs difficult to assess. Even the thickest deformation band clusters is invisible on seismic data, and it is, therefore, impossible to decide whether poor well performance or poor communication between wells is to be explained by deformation bands, subseismic faults, or both. It is also difficult to separate their effect from that of the associated fault core. Calculations and field observations presented by Fossen and Bale [13] indicate that deformation bands only have limited effects on reservoir production unless the bands show unusually high permeability reductions (higher than four orders of magnitude) or occur in very high numbers in the damage zone. The results of their study are in part based on averaging the permeability over a distance of 500 m between an injector and a producer (including a 50 m wide damage zone). The model is one-dimensional and, hence, does not capture the more complex flow pathways that could be generated at a smaller scale. However, Odling et al. [24] suggest that even if the fault core dominates the bulk permeability of the whole fault zone, the contribution of the fault damage zone to the fault sealing capacity cannot be neglected. Sternlof et al. [31] study the flow and transport effects of compaction bands in sandstone. They simulate flow in two-dimensional domains with linear dimensions of several hundred meters, using a discrete-feature model, based on finite-volume approximation. The numerical results show that the presence of deformation bands has an essential impact on the flow. The impact depends partly on the band orientation. These contrasting views show that large uncertainty is still associated with the role of damage zone structures in reservoirs under production. Moreover, in reservoir-scale flow models, where damage zones cannot be modeled explicitly and where major fault zones often are represented by only one grid block, upscaling of the fine scale flow patterns is still a challenge. The ratio between the thickness of the deformation bands (millimeter to centimeter scale) and the computational scale (1- to 10-m scale) may be three to four orders of magnitude. Therefore, upscaling methods are needed [11].

The objective of this work is to develop and study the sensitivity of parameter data on a computational scale, suited for the simulation of flow in fault damage zones. More specifically, we seek to characterize the influence of some properties of deformation band populations on fluid flow in a coarse block (with a size of 1×1 m) and understand how the effective permeability is affected. Focus is on characteristics observed in natural damage zones represented by deformation band populations, notably the orientation of the bands (synthetic or antithetic to the fault core), their clustering, the heterogeneous distribution of permeability along bands, and the variable density of deformation bands in a damage zone. Results are presented in order to illustrate the effect of these different deformation band configurations on the upscaled bulk permeability.

For some parameters, the uncertainty in the geological field measurements is large, leading to a large modeling error. The modeling error is approached through statistical models based on distributions generated from databases and from data given in the literature. Thus, both modeling error and error originating from loss of subgrid information in the upscaling procedure might be evaluated.

2 Deformation band population characteristics in the damage zone

This study focuses on deformation band populations in fault damage zones, and any additional secondary faults or slip surfaces that may exist in the damage zone are not taken into account. We are aware that if such subsidiary faults and slip surfaces are open, permeability within the fracture is enhanced [3, 12, 20], and they could strongly enhance fluid flow in the damage zone by connecting domains that are otherwise separated

by a low permeability zone (such as clusters of deformation bands). These fractures often contribute to fluid flow across the stratigraphic layering. At the same time, slip surfaces are mostly contained in deformation band clusters [19], and the slip planes themselves have thin cataclastic wall rocks of very low permeability. Hence, layer-parallel fluid flow can be expected to be retarded by both deformation band clusters, and these low permeability fracture wall rocks. Moreover, slip planes are generally sparse and unconnected within fault damage zones in highly porous sandstones and only form connected networks in the fault core [24]. We, thus, emphasize our study on the effect of the deformation bands solely.

2.1 Deformation band distribution around the fault core

Fault frequency profiles across fault damage zones show an overall decrease in deformation band density away from the fault core [2, 4, 15, 17, 21, 30]. Based on a comprehensive database consisting of damage zone data from Utah and Sinai (CIPR database), this decrease can be modeled as a logarithmic decline in more than 80% of the cases (Fig. 2). The frequency of deformation bands can, thus, vary from 1 to 200 bands/m (largest extreme value observed in Utah) along a single damage zone, with the maximum density being close to the fault core. If we consider a homogeneous distribution of deformation bands in the damage zone, the average density of deformation band is around 10–15 bands/m, regardless of the fault throw.

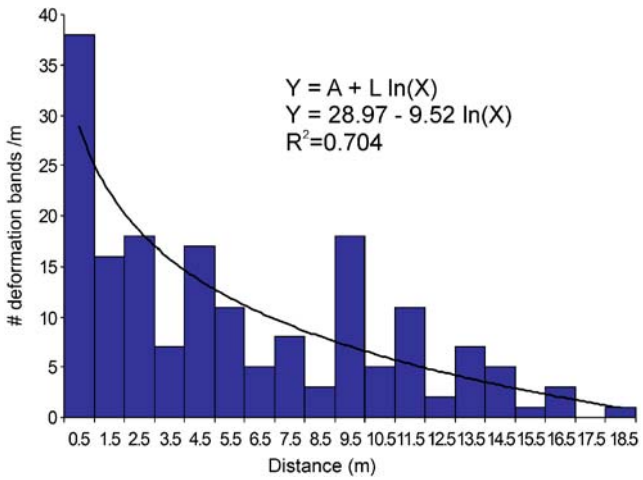

Fig. 2 Decrease of the frequency of deformation bands per meter (Y) in a damage zone in siliciclastic reservoirs. The highest densities are found close to the fault core; however, significantly large cluster of deformation bands also exist at a certain distance of the fault core. X is the distance from the fault core, and R^2 is the fitting factor of the logarithmic decrease to the data

2.2 Spatial distribution of the band in the damage zone

Modeling deformation band density reduction away from the fault core by a logarithmic function is a simplification that does not reflect the tendency of deformation bands to form cluster. The clustering of deformation bands has been characterized by Du Bernard et al. [9] by means of a correlation analysis. The correlation analysis consists of calculating the correlation integral based on the discretized equation of Grassberger and Procaccia [16]. The equation used was adapted as:

$$C(r) = \frac{2}{N \times (N-1)} \sum_{i<j} \Theta\left(r - \left|x_i - x_j\right|\right) \approx r^{\mathrm{Dc}} \qquad (1)$$

where N is the total number of deformation bands in the scan lines, r is the distance, and x is the position of the deformation band in the scan line (distance from the fault core). Θ is the Heaviside function, which is defined as $\Theta(x) = 1$ if $x > 0$, and as $\Theta(x) = 0$ if $x < 0$.

The correlation function corresponds to the relative number of pairs of deformation bands that have spacing lower than a certain distance r. This analysis requires knowledge of the exact position of each deformation band along a scan line in the damage zone. If the distribution of the deformation band is fractal, then the function appears linear in a log–log diagram (Fig. 3A), and its slope corresponds to the correlation dimension Dc. The degree of clustering is, thus, characterized by Dc. For 1D fractal organizations, Dc can vary between 0 (complete clustering) and 1 (no clustering; Fig. 3B). Theoretically, a Dc value of 0 implies all of the deformation bands to be at the same position, and a correlation dimension of 1 corresponds to a homogeneous distribution of deformation bands in the damage zone. Observations of several damage zones of normal faults in sandstones (using the CIPR database) have shown that the average correlation dimension is 0.84 with a standard deviation of 0.06, implying that deformation bands are fractally organized in the damage zone.

2.3 Orientation of the deformation bands

Deformation bands in damage zones generally trend subparallel to the major fault with synthetic and antithetic dips [2, 19, 29], although some may trend oblique to the major fault [12, 20]. Some studies indicate that synthetic and antithetic structures appear to be geologically coeval and in equal proportions for faults with

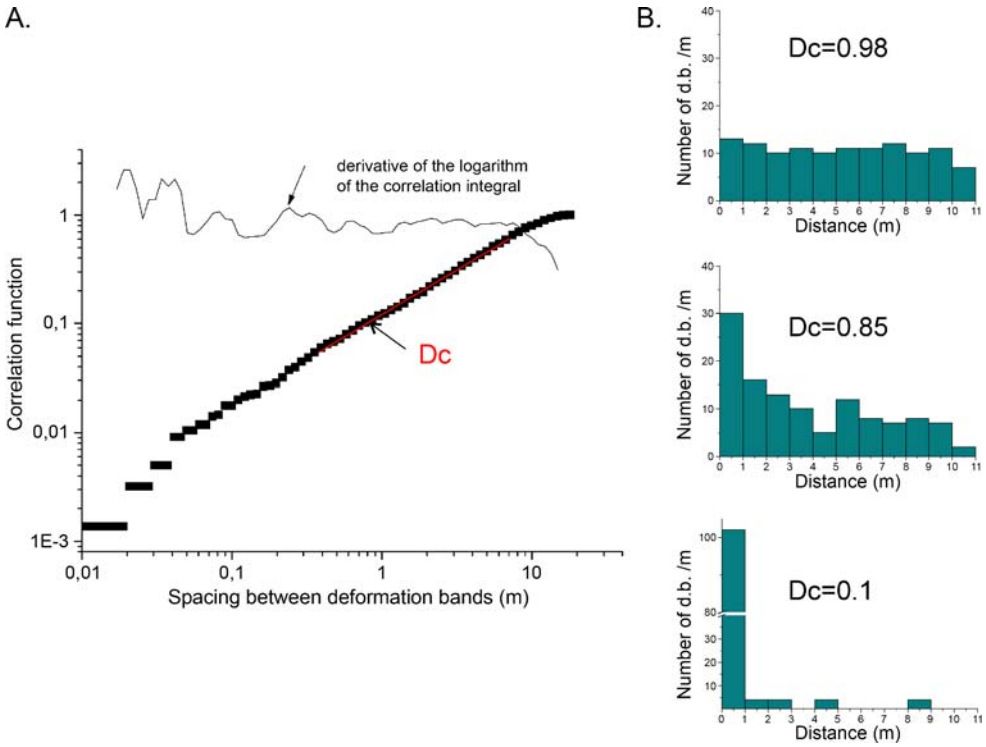

Fig. 3 Correlation analysis: **A** Correlation function as a function of the distance. The slope of this function in a log–log plot corresponds to the correlation dimension. **B** Examples of values of Dc and their corresponding frequency graphs. The organization the closest to the one observed in nature is Dc = 0.85

displacement larger than around 30 m whereas smaller faults show a dominance of synthetic structures [2, 17, 24, 29]. Within the damage zone, the abundance of each set can also vary with location. Within a cluster, the deformation bands have roughly the same dip direction. Considering the correlation of dip direction between two successive deformation bands indicates that two deformation bands have more than 70% chance of having the same dip direction (synthetic or antithetic) if their spacing is less than 10 cm (analysis performed on four scan lines using the CIPR database).

2.4 Petrophysical properties of deformation bands

Cataclastic bands are a common type of deformation bands in fault damage zones, particularly in cases where deformation occurred at depths in excess of 1 km; only this type of bands will be considered in this study. Even if these structures have been widely studied, the precise description of their geometry (length distribution, orientation, spatial continuity) and particularly the variation of their petrophysical properties are still not well known. The thickness of the deformation bands, which typically is around 1 mm [14], varies along many bands. In this study, an average width of 1 mm was chosen. Significant variations in porosity and permeability along selected deformation bands have been documented by Torabi and Fossen [32], but more extensive work is needed to map the frequency and understand the mechanisms responsible for these changes.

3 Numerical method

The solver used in this study is based on a finite volume method and was developed for the numerical solution of the filtration problem. The main computational difficulty of the solution deals with the extremely irregular spatial distribution of the permeability field caused by the existence of complex networks of deformation bands crossing the media. It is possible to assume that the computing complexity of the problem will grow with an increase in number of deformation bands, permeability contrast, or decrease in band's width.

We consider a steady flow through a saturated porous medium. For a stationary 2D flow, we solve the following Darcy law and continuity equation:

$$q = -\frac{1}{\mu} K \nabla p \tag{2}$$

$$\nabla \cdot q = 0 \tag{3}$$

where q is the Darcy velocity, p is the pressure, μ the dynamic viscosity (constant in all the simulations), and K the permeability.

Because of discontinuity of the permeability K, the finite volume method was used with a rectangular grid

for solving the problem. Integrating Eqs. 2 and 3 over the small volume surrounding each node point on a mesh and applying Gauss's theorem, we get the following equation:

$$\iint_{V_k} \operatorname{div}\left[K \operatorname{grad} p\right] dV_k = \int_{S_k = G_{k1} \cup G_{k2} \cup G_{k3} \cup G_{k4}} K \frac{\partial p}{\partial n} dS_k = 0 \tag{4}$$

where V_k is the volume of the cell k, S_k is the surface of the cell k, and G_{k1}, G_{k2}, G_{k3}, and G_{k4} represent the cell boundaries (Fig. 4).

The derivative on boundaries G_{ki} in Eq. 3 was approximated using the work of Marchuk [23]. For example, the flow rate through G_{k4}:

$$Q_{k-1/2} = \int_{G_{k4}} K \frac{dp}{dn} dS_{k4} \approx \frac{p_k - p_{k-1}}{\int_{[X_{k-1}, X_k]} \frac{1}{K} dx} A, \tag{5}$$

where A is the length of G_{k4}, $\left[X_{k-1},\ X_k\right] \perp G_{k4}$ (Fig. 4), p_k is the pressure in the middle of the cell k, and $Q_{k-1/2}$ is the flow rate through G_{k4}.

Thus, we have a so-called dual-grid structure. The first grid consists of a set of S_k boundaries of control volumes V_k. The second grid consists of a set of X_k—centers of control volumes V_k. For correct flow simulation the second grid X_k should be chosen so that each body included in its cell should intersect at least one boundary of this cell.

We solve Eqs. 2 and 3 by using the approximation (5) in the domain $D = \{0 \le x \le L_x,\ 0 \le y \le L_y\}$. The host rock has a permeability of 1 darcy. Each upscaled block has a size of 1 × 1 m. By default, a rectangular grid contains 80 × 80 nodes for one upscaled block, and each deformation band corresponds to a 1 mm thick band with a default permeability of 10^{-2} darcy. The representation of thin deformation bands in a numerical model is a rather difficult problem. Therefore, the method of integral identities [23] was applied to solve the problem with discontinuous permeability coefficient. In our model, the integral on the right side of Eq. 5 is computed analytically because permeability is a piecewise function with known borders. Therefore, the solution of Eq. 5 is exact in 1D even if the width of the bands is much smaller than the grid size. In 2D, some errors are introduced in the solution because the bands are not parallel to the grid. The accuracy of the solution was verified by comparing analytical results with results obtained on highly resolved models. The numerical tests presented in Fig. 5 show that the results of the calculations do not change significantly when the numerical resolution is increased. In these tests, the flow rate is computed by using 40 × 40, 80 × 80 and 260 × 260 grid nodes for 20 random realizations of deformation band distributions (Fig. 5). Here, Dc = 0.8, $I_\theta = 0$, and the number of deformation bands is $N = 10$ (see Section 5 for the meaning of the different parameters). On two opposite boundaries, we set fixed pressures $P_1 = 2$ Pa and $P_2 = 1$ Pa, whereas no flow boundary conditions apply to the other borders (see Fig. 7 for model setup). The relative difference between the curves corresponding to 80 × 80 and 260 × 260 nodes is less than 2%. We consider, thus, that the thin deformation bands are accurately resolved in the chosen grid (80 × 80 nodes).

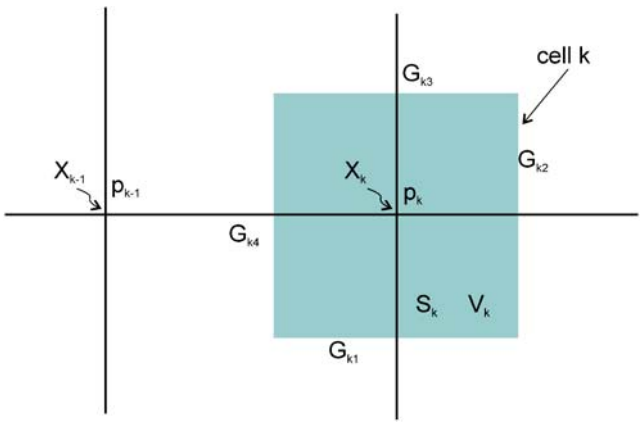

Fig. 4 Method of calculation based on the finite volumes method. Sketch of a cell k with center point X_k, volume V_k, surface S_k, and pressure p_k at X_k. G_{k1}, G_{k2}, G_{k3}, andG_{k4} are the boundaries of the cell k

Furthermore, a statistical approach is used to study the flow in the damage zone. In this work, we construct a model describing a deformation band's population in the damage zone. Due to strongly irregular band structures, we assume that several geometrical parameters of this model are random functions. Therefore, the permeability field is also considered as a random field described completely by the probability distribution of random parameters. Then, any flow characteristic ξ (flow rate, velocity, effective permeability, etc.) also becomes a random function. This approach allows us to compute averaged flow characteristics only. Having the ensemble of the random parameters' realizations sampled accordingly with the correspondent distribution, we can calculate the value of flow characteristic ξ_i for each realization as well as the effective properties by using the following statistical averaging:

$$E\xi \approx \langle \xi \rangle = \frac{1}{N_S} \sum_{i=1}^{N_s} \xi_i \tag{6}$$

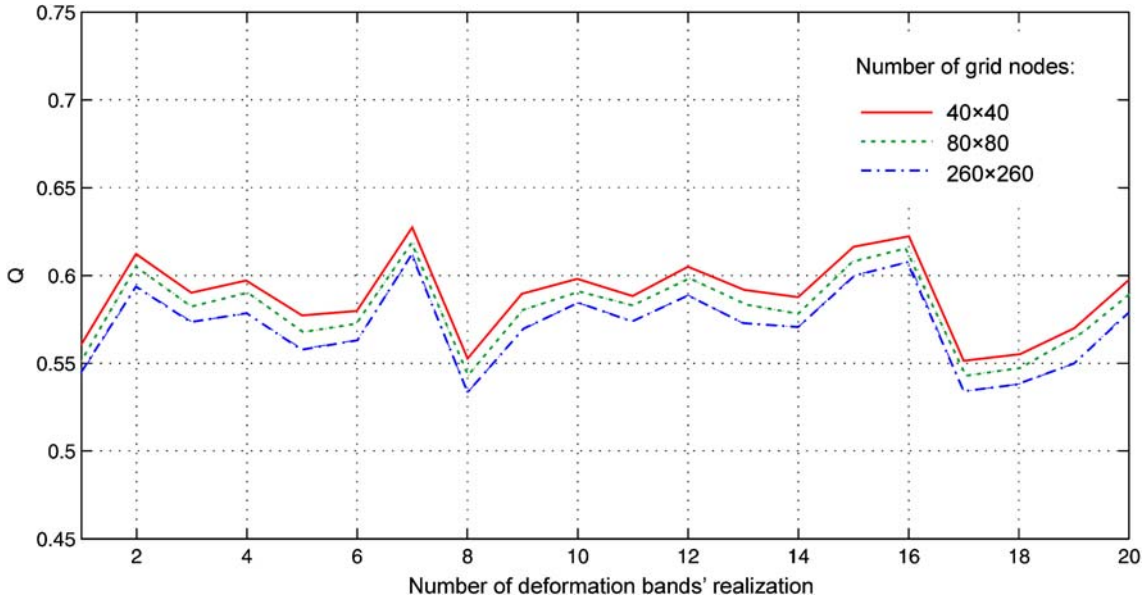

Fig. 5 Flow rate computed by using 40 × 40, 80 × 80, and 260 × 260 grid nodes for 20 random realizations of deformation band population, $N = 10$ deformation bands; Dc = 0.8, $I_\theta = 0$, dip $= \pi/3$, $K_{DB}/K_{HR} = 0.01$. On two opposite boundaries, we set the fixed pressures $P_1 = 2$ Pa and $P_2 = 1$ Pa, whereas no flow boundary conditions apply to the other borders. The relative difference between the two curves "80 × 80" and "260 × 260 nodes" is less than 2%

with N_S as the number of realizations. Here, $\langle\,\rangle$ means the ensemble averaging.

In Monte Carlo methods, the evaluation of the statistical error $\nu(\xi)$ is essential. The standard estimation has the following form [27]:

$$\nu(\xi) = \alpha(\beta)\,\frac{\sigma_\xi}{\sqrt{N_S}} \tag{7}$$

where α is a coefficient depending on the confident coefficient β. For example, $\alpha(0.997) = 3$ and $\alpha(0.95) = 1.96$. σ_ξ is the standard deviation of random value ξ. The number of realizations used in all our Monte Carlo simulations is $N_S = 1{,}000$.

4 Upscaling

As noted previously, geological models frequently incorporate heterogeneities on the scale of a few centimeters and can contain in the order of 10^7 grid cells (e.g., [24, 25]). However, current flow simulators are technically limited to 10^4 to 10^5 cells, with grid cells typically being a few hundred meters horizontally and a few tens of meters vertically. Upscaling methods are, thus, required for flow modeling. The aim of upscaling is to reproduce the global behavior of the reservoir but still capture the local behavior, and the challenge is to transfer the geological information to the coarser cells without losing crucial information existing at the finest scale.

A large number of papers have been devoted to different upscaling techniques. A good survey of different methods is presented in [11] and reviews are found in [22, 24, 26, 28]. In general, these different approaches can be divided in two main groups: local approaches [5, 10, 25] and global ones [6, 18]. In the local methods, the upscaled permeability of the coarse blocks only depends on the real media permeability inside each block (pure local upscaling) and on the permeability of the surrounding area (extended local upscaling). By contrast, global and quasi-global methods utilize the fine-scale permeability on the whole domain for the calculation of the upscaled permeability for each coarse block.

The advantage of global upscaling is that the information about the fine-scale permeability in the entire domain is used for flow computation. However, the main shortcoming of the global upscaling is an extremely large computational cost. Therefore, for the numerical solution of the flow problem in whole domain, we apply the adaptive local–global upscaling (ALG) [7]. The ALG procedure is briefly described in part 6.3, and an example of numerical computations is given.

For the sake of simplicity, the effect of deformation band populations on fluid flow will be mainly studied for a diagonal upscaled permeability tensor. On two

opposite boundaries, the pressures are fixed to constant values P_1 and P_2, whereas no flow boundary conditions apply to the other borders (example in Fig. 7). A flow calculated numerically allows us to estimate the effective permeability K_{eff} of a coarse upscaled block D from equation [26]:

$$\langle q \rangle = -\frac{1}{\mu} K_{\text{eff}} \langle \nabla p \rangle . \tag{8}$$

1,000 realizations of deformation bands configuration are sampled according to the procedure described below. Then, the mean values for the flow rate and pressure gradient are estimated by using a local upscaling method. Finally, K_{eff} is calculated. In this upscaling procedure, the averaged upscaled permeability K^{ups} is a positive definite diagonal tensor, where diagonal elements are equal to the effective permeability K_{eff} in x and y directions. Strictly speaking, we use in this paper an extended local upscaling. The linear size of the extended domain between boundaries with Dirichlet boundary conditions is equal to the size of the coarse block plus one grid cell size.

Diagonal K^{ups} may not give accurate quantitative results, but we expect that the results are well suited for the sensitivity analysis. Some of these calculations are repeated in a 2D upscaling framework where K^{ups} is a full positive definite tensor. We aim at showing that the trends obtained with diagonal K^{ups} for the effect of some characteristics of the deformation band distribution are qualitatively similar in the upscaling method with full K^{ups}. Finally, we deal with the upscaling problem in the global domain and emphasize the advantage of the adaptive local–global upscaling in comparison with the pure local upscaling.

5 Parameters tested

One of the problems considered in this study is the influence of deformation band distribution on flow in the damage zone. Based on the modeling presented in the previous section, we will upscale the effects on flow in the damage zone based on the following parameters:

- Spatial distribution of the bands (i.e., clustering)
- Orientation of the deformation bands
- Heterogeneity of the petrophysical properties of the deformation bands
- Variation in band density.

The sensitivity of these different parameters is of special interest in defining the effective permeability related to damage zones in porous sandstones.

The clustering of the deformation bands is characterized by the correlation dimension Dc defined by Eq. 1. Since only a 1D fractal organization is taken into account in these simulations, the correlation dimension Dc is varied between 0 and 1. The following values are particularly tested: 0.2, 0.5, 0.8, and 1. Furthermore, in considering upscaling in the domain D, we assume that all deformation bands intersect the segment Z connecting the points with coordinates $(0.5L_x, 0)$ and $(0.5L_x, L_y)$. Using the procedure described below, a set of bands' centers $\{C_i\} \in Z$ is sampled according to chosen Dc under the condition $|C_i - C_j| > d$, $\forall i, j$, and d being the width of each deformation band. In our simulations, d is equal to 1 mm.

In this work, for simulating the set of points with a given correlation dimension Dc in 1D, we use multiplicative cascade processes [16]. In 1D, the recursive algorithm described in Darcel et al. [8] is used. As a result of this algorithm, we get a subdivision $Z = \{Z_1, Z_2, \ldots, Z_M\}$ for the entire domain $(Z = Z_1 \cup Z_2 \cup \ldots \cup Z_M)$ and the corresponding set of probabilities $P = \{p_1, p_2, \ldots, p_M\}$ such that $(p_1 + p_2 + \ldots + p_M = 1)$. When Z and P are constructed, we distribute each deformation band center C_i randomly and mutually independently in one of the subdomains Z_j according to the probabilities $\{p_j\}$ by using the Monte Carlo method. On each iteration, each Zj is divided in two equal parts. The iteration procedure can be repeated infinitely, but in our simulations, we used a number of iterations T between 5 and 7 producing M subdomains $(M = 2^T)$.

The computing rule of P is illustrated briefly in Fig. 6. Each element of P has the form

$$q_1^l \, q_2^{T-l}, \quad 0 \le l \le T.$$

The set P involves C_T^l elements. Here, q_1 and q_2 are calculated from [8]:

$$q_1 + q_2 = 1 \quad \text{and} \quad \frac{q_1^2 + q_2^2}{(1/2)^{\text{Dc}} = 1}.$$

If we assume an isotropic cascade process, the pair of probabilities corresponding to the two parts of the divided subdomains can be randomly permuted. Thus, for each element of the ordered set Z, we construct the corresponding element in the ordered set P. The distribution of deformation bands along a 1D scan line will, thus, reproduce a clustered or fractal organization characterized by the correlation dimension Dc.

Each band is characterized by its dip (angle between the horizontal and the band). Only the sense of dip (toward the left or the right) is varied in this study. Furthermore, each deformation band crosscuts the whole model. The distribution of the orientations

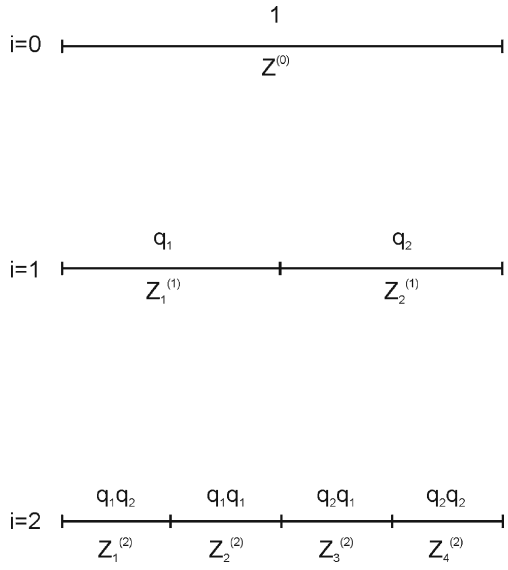

Fig. 6 Hierarchical construction of a fractal set points. $Z_j^{(i)}$ is the length of the jth subdomain of the domain Z at the ith iteration. q_1 and q_2 are the probabilities of finding one point in one subdomain so that $q_1 + q_2 = 1$

can be random and correlated with a specific correlation coefficient, described hereafter.

In some models, the angle between the deformation bands and the boundaries with fixed pressure is $\theta_i = \pm\pi/6$ (complementary angle of the dip). We assume that $\{\theta_i\}$ is the set of random variables ordered by the y coordinate. Let the sign of θ_1 be chosen randomly according to the equal probability $p = 0.5$ for $\pi/6$ and $-\pi/6$. The orientation of the other deformation bands is then defined recursively. If two neighboring bands have their centers in the positions Y_{i-1} and Y_i and the orientation of the first band is known, then the second band has a same orientation with a probability of:

$$p(r) = p(Y_{i-1}, Y_i) = \frac{1}{2}\left(1 + \exp\left(-\alpha \times r\right)\right)$$
$$\text{with } r = |Y_{i-1} - Y_i|$$

The correlation coefficient (radii) is defined as:

$$\rho_\theta(\theta_{i-1}, \theta_i) = \frac{E(\theta_{i-1}\theta_i)}{\sqrt{E\theta_{i-1}^2}\sqrt{E\theta_i^2}} = \exp(-\alpha r)$$

where $E\theta_{i-1} = E\theta_i = 0$ and $I_\theta = 1/\alpha$. I_θ is the correlation length of the random field θ.

The correlation length I_θ was varied between 0 and 0.2 m. The correlation length characterizes the distance below which two bands will have a correlated orientation (same dip direction). In the case where $I_\theta = 0$, the orientations of the deformation bands are statistically independent.

As observed in nature, the permeability inside a deformation band is not necessarily constant and homogeneous. In some simulations, holes are introduced in the bands. It means that a certain length of the deformation band presents an increased permeability in comparison with the rest of the band. In our simulations, an average permeability contrast between the band and the host-rock of around 10^{-2} is fixed. Hence, if we consider a deformation band with a permeability K_{DB} of 0.001 darcy, the holes having a permeability K_{hole} of 0.091 darcy and the total length of the holes in each deformation band being 10 cm, then the perpendicular average permeability of the band $K_{\mathrm{DBaverage}}$ is calculated as the arithmetic average $\frac{(L-h)\times K_{\mathrm{DB}} + h \times K_{\mathrm{hole}}}{L}$ (with L, the length of the deformation band—here 1 m—and h the total length of the holes) and equals 0.01 darcy. Four configurations are tested: a single hole having the same position in each deformation band, a single hole with a random position, eight uniformly spaced holes with a total length of 9 cm, and eight holes randomly spaced (Fig. 10). In all the simulations, the host rock permeability K_{HR} was fixed to 1 darcy.

The deformation band frequency is not constant in the damage zone but decreases away from the fault core. Six densities were tested: 5, 10, 15, 25, 30, and 60 deformation bands per meter. The default frequency is 10 deformation bands in each upscaled block.

6 Numerical results

6.1 Local upscaling: diagonal permeability tensor

6.1.1 Reference bulk-effective permeability

If the deformation bands are oriented perpendicular to the flow direction and if they present a constant permeability, the flow along a grid element perpendicular to the bands can be calculated analytically [13, 24]. In this case, the bulk permeability corresponds to the harmonic average of the permeabilities crossed by the flow:

$$K_{\mathrm{ref}} = \frac{\sum_{i=1}^{N} l_i}{\sum_{i=1}^{N} \frac{l_i}{k_i}} \tag{9}$$

where l_i is the thickness of the different domains crossed by the flow, k_i the corresponding permeability, and N is the number of existing domains. This value is independent of the clustering of the deformation bands in the media and was used as a reference value.

6.1.2 Role of the orientation of the deformations bands and their clustering

In the simulations presented in Fig. 7, the bands present a homogeneous constant permeability of 10^{-2} darcy. Ten bands are considered in the upscaled block. The deformation bands are dipping 60° either toward the left or toward the right. We consider here a variable correlation coefficient I_θ between the orientations of the dips as described above (parameters tested).

Figure 7 presents the bulk-effective permeability K_{eff} in the upscaled coarse block as a function of the correlation dimension Dc and various correlation lengths for the orientation of the band dips. The gray line corresponds to the analytical average bulk permeability K_{ref} for bands perpendicular to the flow direction.

For a specific clustering, increasing the correlation length increases the bulk-effective permeability. Varying the clustering of the bands has a negligible effect when the orientations of the bands are mutually independent ($I_\theta = 0$ m). If the correlation length between the orientations of the bands is strong (i.e., over a certain length, the bands have the same orientation), increasing the clustering of the bands (by decreasing Dc) leads to a slight increase in the bulk permeability. The correlation between the dip orientations has however not a strong effect on the effective permeability in the system: even for a strong clustering (low Dc) and for I_θ varying between 0 and 0.2 m, the variation of the effective permeability is less than 0.03 (~5%).

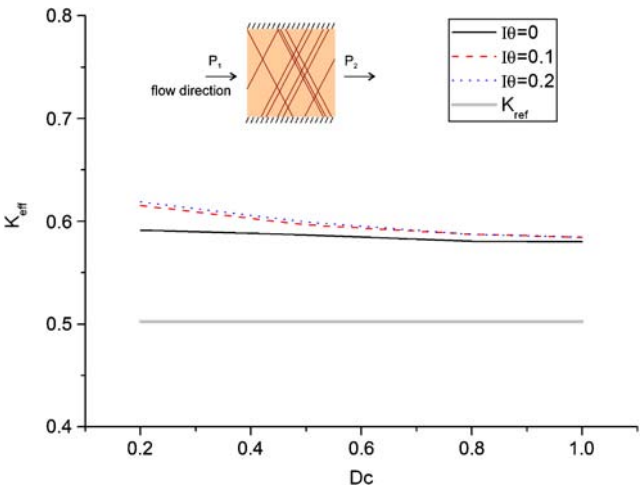

Fig. 7 Effective permeability K_{eff} in the upscaled coarse block as a function of the correlation dimension Dc for various correlation lengths I_θ of the dip orientations. K_{ref} is the reference permeability calculated for continuous deformation bands perpendicular to the flow direction

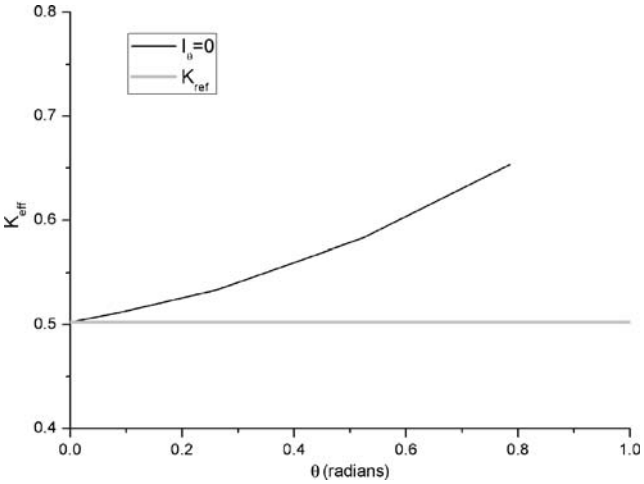

Fig. 8 Effective permeability K_{eff} in the upscaled coarse block as a function of the dip of the deformation bands $(\text{dip} = \pi/2 - \theta)$. $I_\theta = 0$ (random orientation of the dip), number of structures = 10; permeability contrast between the bands and the host rock: 10^{-2} and Dc = 0.8. K_{ref} is the reference permeability calculated for continuous deformation bands perpendicular to the flow direction, corresponding to $\theta = 0$ or a dip equal to 90°

Actually, the difference between the curves $I_\theta = 0.1$ m and $I_\theta = 0.2$ m is comparable with the statistical errors of the numerical calculations.

Varying the dip of the deformation bands also influences the effective permeability in the block (Fig. 8): The more parallel to the flow direction the bands are, the higher the effective permeability. As expected, flow along rather than across the deformation bands will be favored.

Decreasing the deformation band permeability (K_{DB}) decreases the effective permeability in the system. Moreover, we note that the effect of clustering and correlation of dip orientation becomes stronger when the permeability contrast increases (Fig. 9). For clustering characterized by large correlation dimensions (Dc = 0.8–1), the effect of the clustering has only a small effect on the effective permeability in the upscaled block.

6.1.3 Effect of heterogeneous petrophysical properties along the bands combined with variation in clustering

In these simulations (Fig. 10), the deformation bands are perpendicular to the flow direction. A heterogeneous distribution of permeability inside each band is now considered. In order to simplify the configuration of the simulations, we first consider a 10-cm "hole" per band having permeability K_{holes} of 0.091 darcy; the permeability in the rest of the band K_{DB} being equal to

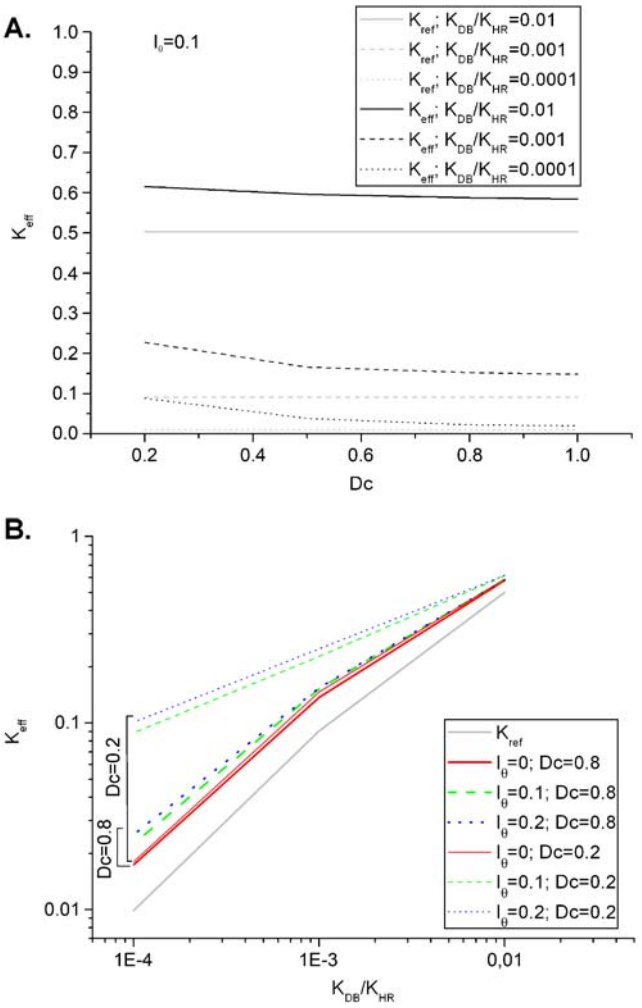

Fig. 9 **A** Effective permeability K_{eff} calculated in the upscaled block and reference permeability K_{ref} if the bands are perpendicular to the fluid flow as a function of the correlation dimension Dc. Different permeability contrasts $K_{\text{DB}}/K_{\text{HR}}$ are tested; K_{DB} is the permeability in the deformation band, and K_{HR} is the permeability in the host rock. Number of deformation bands = 10; $I_\theta = 0.1$. **B** Effective permeability K_{eff} as a function of the permeability contrast $K_{\text{DB}}/K_{\text{HR}}$ for various correlation length of dip orientation I_θ and various correlation dimensions Dc

10^{-3} darcy. The average permeability across the band is equal to 10^{-2} darcy by considering a flow strictly perpendicular to the band, which does not capture the 2D nature of the flow. In this case, two reference values were calculated: the one without holes "K_{ref} for $K_{\text{DB}}/K_{\text{HR}} = 0.001$" and the one taking into account the holes "K_{ref} for $K_{\text{DB}}/K_{\text{HR}} = 0.01$."

The first configuration tested is the case where the holes have exactly the same position in all the bands, implying that the holes are aligned parallel to the flow direction (Fig. 10, 1h-uniform). In this case, increasing the clustering of the bands increases the bulk permeability in the band (Fig. 10, curve 1h-uniform).

In nature, the probability of having holes aligned parallel to the flow direction is rather low, unless the holes are controlled by stratigraphic heterogeneities within the layer. Therefore, a second configuration was tested in order to randomly position the hole on each deformation band (Fig. 10, 1h-random). This random configuration reduces the general bulk permeability in the block in comparison with the uniform one. Moreover, increasing the clustering (by decreasing Dc) in that case leads to an additional decrease of the bulk-effective permeability, contrary to the uniform case.

Because deformation band heterogeneities can occur repeatedly along bands at the microscale [13], a third configuration was explored, where the single deformation band hole was replaced by eight smaller holes of the same total length (10 cm). In this configuration, the hole length (1.25 cm) is larger that the grid step (1.23 cm). The results indicate that this fragmentation of the permeability heterogeneity globally increases the bulk-effective permeability in the block. If the holes are randomly distributed on each band (Fig. 10, curve 8h-random), then increasing the clustering decreases the bulk-effective permeability. On the contrary, if the holes are uniformly positioned, then increasing the clustering (by decreasing Dc) increases the bulk-effective permeability K_{eff}.

Comparing the difference in bulk-effective permeability K_{eff} as a function of the clustering for the cases above (uniform and random positions of the holes and for only one large heterogeneity and for a fragmented heterogeneity) indicates that clustering has a lower effect on bulk-effective permeability than the distribution of permeability anomalies in the deformation bands. It is also interesting to note that assigning an average constant permeability to the band such as "K_{ref} for $K_{\text{DB}}/K_{\text{HR}} = 0.01$" leads in that case to an overestimation of the effective permeability in the coarse block.

6.1.4 Effect of deformation band density

Deformation band density is varying within the damage zone and is globally decreasing when moving away from the fault core. In Fig. 11, the effect of variable density is tested in combination with the effects of clustering and orientation. As expected, the effective permeability decreases with increasing deformations band density in each coarse block. The results indicate that for densities higher than 10 deformation bands per meter, the effective permeability in the coarse block is reduced at least by 50% compared to the host rock permeability, if we consider deformation bands having a constant permeability of 0.01 darcy and being perpendicular to the flow direction (curve K_{ref} in Fig. 11).

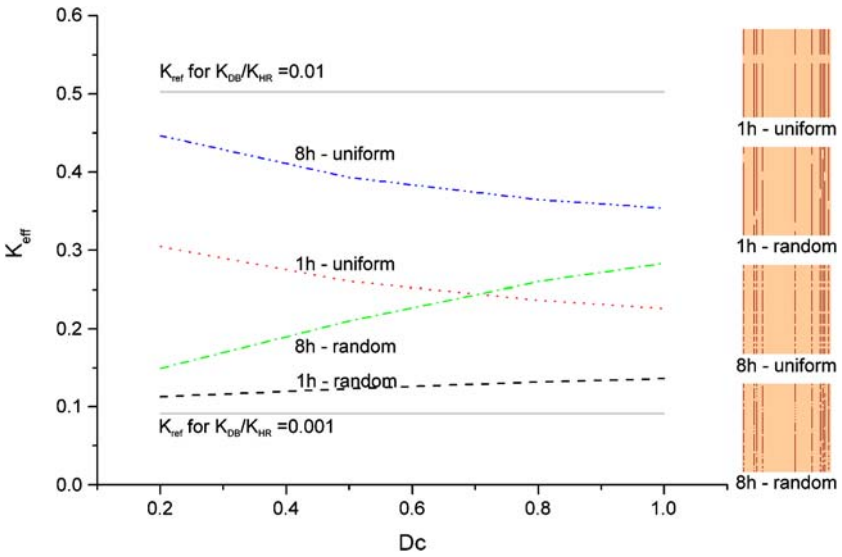

Fig. 10 Effects of permeability discontinuities along the deformation bands (10 deformation bands perpendicular to the flow direction). $K_{\mathrm{DB}} = 0.001$ and $K_{\mathrm{holes}} = 0.1$. The total length of holes in each deformation band is equal to 9 cm in all the simulations. The different configurations tested are: *1h-uniform* only one hole placed in a similar position along the bands in all the bands; *1h-random* only one hole placed randomly along the band; *8h-uniform* eight holes placed similarly in all the bands; *8h-random* eight holes placed randomly along the bands. The two *gray curves* correspond to the analytical solution for ten bands with a uniform permeability: the *lower curve* corresponds to bands having a permeability of 0.001, and the *upper* one to bands having a permeability of 0.01 (which is average across band permeability of the band with the holes)

If we consider deformation bands with ±60° dip (and Dc = 0.8, $K_{\mathrm{DB}} = 0.01$ darcy), a density of 15 deformation bands is required to reduce the effective permeability by 50%. The correlation of the dip orientations has no real influence on the effective permeability if the correlation dimension Dc is large (0.8–1). For lower Dc, the influence of the correlation of dip orientation has to be taken into account.

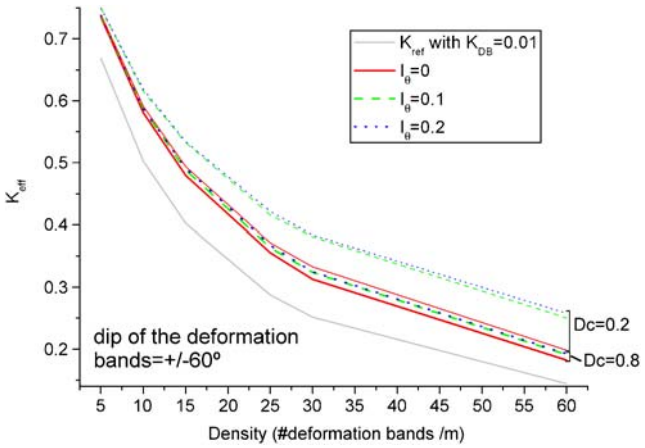

Fig. 11 Effective permeability K_{eff} in an upscaled block as a function of the density of deformation bands (number of deformation bands in block of 1 m long; $K_{\mathrm{DB}} = 0.01$) . The reference permeability K_{ref} corresponds to deformations bands being perpendicular to the flow direction and having a constant permeability. Two types of clustering have been tested characterized by a correlation dimension Dc equal to *0.2* (strong clustering) and *0.8* (weak clustering), respectively

6.2 Local upscaling: full permeability tensor

In this paragraph, we deal with 2D extended local upscaling. Here, for each geological realization, we solve two problems with fixed pressure on two opposite boundaries and linear pressure variation on the other boundaries parallel to the main flow direction [11]. The resulting upscaled permeability is a positive definite full tensor. The upscaled coarse block here has a size of 1 × 1 m and the total number of the inner nodes in the coarse block is 80 × 80. The linear size of the extended domain is equal to the size of the coarse block plus one grid cell size.

In Table 1, we study the significance of off-diagonal terms of the upscaled permeability tensor. In the first row, the relations $\left|K_{xy}^{\mathrm{ups}}\right| / K_{xx}^{\mathrm{ups}}$ and $\left|K_{xy}^{\mathrm{ups}}\right| / K_{yy}^{\mathrm{ups}}$ are shown for $N = 10$, Dc = 0.8, $|\theta| = \pi/6$ and $I_\theta = 0$ m. Twenty thousand realizations of the distribution of the deformation bands were sampled. In the next rows, we stepwise change one of these parameters to compare the results. Here, we present the percentage of realizations for which these ratios were greater or equal to 5%, 10%, 15%, and 20%, respectively. Note that the relative value of the off-diagonal terms grows with

Table 1 Influence of different parameters of the model on the relation between off-diagonal and diagonal terms of the upscaled permeability tensor

	$\frac{\lvert K_{xy}^{\text{ups}}\rvert}{K_{xx}^{\text{ups}}}, \frac{\lvert K_{xy}^{\text{ups}}\rvert}{K_{yy}^{\text{ups}}} \geq 0.05$	$\frac{\lvert K_{xy}^{\text{ups}}\rvert}{K_{xx}^{\text{ups}}}, \frac{\lvert K_{xy}^{\text{ups}}\rvert}{K_{yy}^{\text{ups}}} \geq 0.1$	$\frac{\lvert K_{xy}^{\text{ups}}\rvert}{K_{xx}^{\text{ups}}}, \frac{\lvert K_{xy}^{\text{ups}}\rvert}{K_{yy}^{\text{ups}}} \geq 0.15$	$\frac{\lvert K_{xy}^{\text{ups}}\rvert}{K_{xx}^{\text{ups}}}, \frac{\lvert K_{xy}^{\text{ups}}\rvert}{K_{yy}^{\text{ups}}} \geq 0.2$
	47.2%, 59.1%	15%, 27.3%	2.7%, 9.6%	0.2%, 2.3%
$\theta = \pm\pi/4$	60.5%, 60.6%	29.3%, 29.6%	10.7%, 11%	3%, 3.1%
$N = 20$	44.8%, 60.4%	12.4%, 29.9%	2%, 11.5%	0.17%, 3.5%
$\text{Dc} = 0.2$	36.4%, 49%	8.1%, 18%	1%, 5.1%	0.07%, 1.1%
$I_\theta = 0.1$	73%, 78.7%	46.7%, 57.8%	24.3%, 38.6%	7.9%, 22.1%

20,000 realizations of deformation band distributions were sampled. The reference model (first row) has the following parameters: $N = 10$, $\text{Dc} = 0.8$, $|\theta| = \pi/6$, $I_\theta = 0$ m

increasing $|\theta|$. The ratios grow also with increasing permeability contrast and correlation length of band orientation I_θ. On the other hand, the clustering (decreasing of Dc) decreases the relative value of the off-diagonal terms. At the same time, it seems that increasing the band density is not important for the significance of the off-diagonal terms: the difference between $N = 10$ (number of bands) and $N = 20$ does not exceed the statistical error.

The numerical results presented in Fig. 12 are similar to the curves in Fig. 7. The resulting average upscaled permeability is an average of permeabilities computed by extended local upscaling for $N_s = 1{,}000$ realizations. The curves presented in Fig. 12A are higher than the corresponding curves in Fig. 7. The higher value observed for the permeability is caused by the different boundary conditions. However, for $I_\theta = 0$ and 0.2 m, the relative difference does not exceed 5.5% and 12.5%, respectively, even for $\text{Dc} = 0.2$. The nondiagonal tensor element K_{xy}^{ups} can change sign. Therefore, the averaged value $<K_{xy}^{\text{ups}}>$ is small in comparison with $<K_{xx}^{\text{ups}}>$ and $<K_{yy}^{\text{ups}}>$ and does not exceed 0.006 darcy. Thus, the averaged upscaled permeability tensor is practically diagonal for our model, as the diagonal terms are of the order of unity.

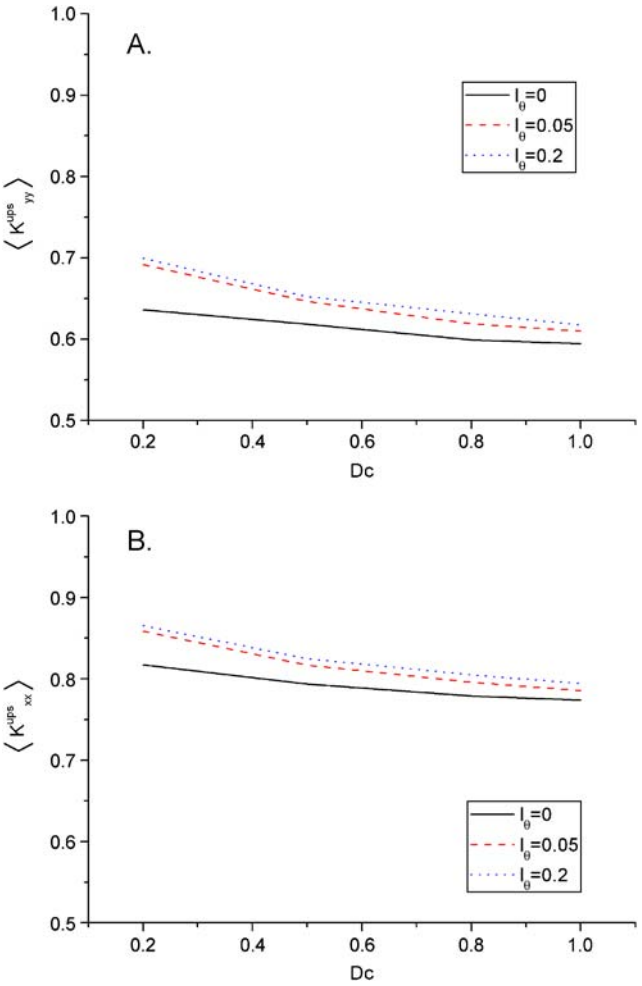

Fig. 12 Simulations using 2D extended local upscaling: influence of the correlation length I_θ on the dip orientations. Number of bands = 10; the permeability in the deformation bands K_{DB} is 0.01, the permeability in the host rock $K_{\text{HR}} = 1$. **A** $<K_{yy}^{\text{ups}}>$ (averaged upscaled permeability in the coarse block along the y axis—at 60° of the deformation band) as a function of the correlation dimension Dc. **B** $<K_{xx}^{\text{ups}}>$ (averaged upscaled permeability in the coarse block along the y axis—at 30° of the deformation band) as a function of the correlation dimension Dc

6.3 Adaptive local–global upscaling

We have mentioned above the procedure of the adaptive local–global upscaling. Following Chen and Durlofsky [7], we prefer the transmissibility upscaling. The basic idea of this iterative procedure is to use the pressure obtained from a global coarse scale solution for the calculation of the local properties. At the first step, the coarse flow transmissibility is calculated by using an extended local upscaling. Furthermore, the global coarse scale pressure is calculated and used for the determination of local boundary conditions. Then, these boundary conditions are used for calculating local properties on the next iteration. The convergence

criterion was chosen as a measure of the differences in pressure and flow rate from one iteration to the next.

We consider a simple model, where the square rectangular domain D consists in 4 × 4 equal coarse blocks and an extended area (Fig. 13). Each block has linear sizes equal to 1 × 1 m, $L_x = L_y = 5$ m. There are 50 deformation bands having a width of 0.001 m distributed in D according to Dc = 0.8 and $I_\theta = 0$ m. The pressures in the corners are $P(0,0\text{ m}) = 1$ Pa, $P(5,0\text{ m}) = P(0,5\text{ m}) = 2$ Pa, $P(5,5\text{ m}) = 3$ Pa. The pressures on the boundaries are fixed and are defined as a linear function between the pressures in the corresponding corners.

In Fig. 14, we present the result for accuracy of the upscaled characteristics. The coarse grid pressure Pc is calculated in blocks centers X_k, and Q_x, Q_y are the flow rates in x and y directions calculated on the corresponding inner boundaries. The measure of accuracy is based on a comparison of the coarse block results with the results of fine scale simulations $\left(P_c^{\mathrm{f}},\ Q_x^{\mathrm{f}},\ \text{and}\ Q_y^{\mathrm{f}}\right)$ and is defined as $\frac{\|P_c - P_c^{\mathrm{f}}\|}{0.5\left(\|P_c\| + \|P_c^{\mathrm{f}}\|\right)}$. The method converges after a few iterations. The relative error for P_c, Q_x, Q_y are about 0.5%, 21%, 29%. For comparison, on 0th iteration, the accuracies of the extended local upscaling are 0.9%, 54%, 67%, respectively. These results indicate as expected that some types of multiscale method should be used to obtain sufficient accuracy in specific applications. For comparison in Fig. 14, we present the results of local–global upscaling. We address the same model as given above, but we divide the computational region into 10 × 10 coarse grid blocks. The total number of fine grid nodes is the same. It is natural that relative error decreases to 0.25%, 16.5%, and 24%, respectively.

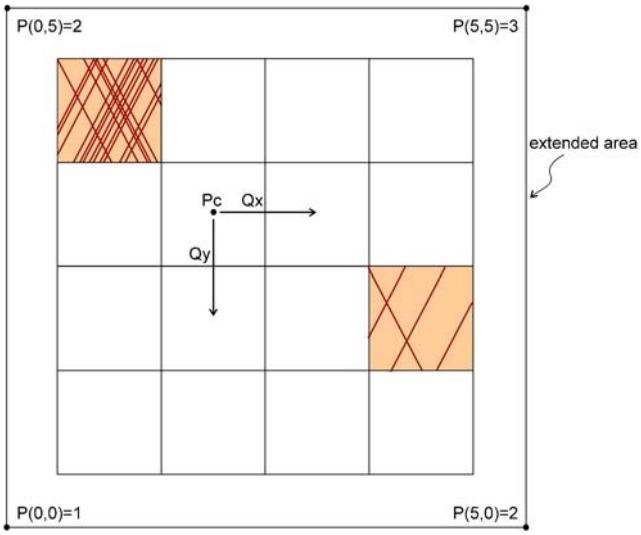

Fig. 13 Test model for the 2D local–global upscaling. The global boundary conditions are given by the pressures at the corners of the extended area and linear function in between. Each coarse block has a size of 1 × 1 m. The flow rates Q_x and Q_y are calculated across the block boundaries, and the coarse block pressure P_c is calculated in the middle of the block

6.4 Probability density of the upscaled permeability

The influence of the model parameters has been studied previously only for average upscaled permeabilities. But it is also interesting to estimate some more complex statistical characteristics like variance or correlation function. It allows us to assess an error of the global upscaling when the effective permeability is used as coarse block permeability. Also, it allows to check the accuracy of statistical averaging by using Eq. 7.

In Fig. 15, 3,000 realizations of deformation band networks have been sampled in order to estimate the probability density of the y component of diagonal upscaled permeability tensor K^{ups} in a coarse block of one meter by 1 m. The following parameters have been chosen: a density of 10 deformation bands per meter, $K_{\mathrm{DB}}/K_{\mathrm{HR}} = 0.01$, Dc = 0.8, and $\theta = \{\pi/6, -\pi/6\}$. For $I_\theta = 0$, 0.1, and 0.2 m, the effective permeability (averaged upscaled permeability) $< K_{yy}^{\mathrm{ups}} >$ is equal to 0.5806, 0.5875, and 0.5872; the mean deviation $\sigma\left(K_{yy}^{\mathrm{ups}}\right)$ being equal to 0.026, 0.030, and 0.032, respectively. Figure 15 presents the density of the random value K_{yy}^{ups}. It points out that the distribution is essentially non-Gaussian, but the results for $I_\theta = 0.1$ and 0.2 m are comparable apart from the statistical error.

7 Discussion—concluding remarks

7.1 Computational method

A 2D statistical model of fault damage zone architecture, incorporating the characteristics of deformation band populations observed in natural examples, has been built in order to investigate fluid flow and permeability upscaling in fault damage zones containing deformation bands. The finite volume method developed for the numerical flow computation allows to use a fine mesh with mesh size larger than the thin width of deformation bands. This method was used for simple 2D rectangular domains with the main flow being parallel to the borders. Numerical tests show that our method keeps the conservation law with high accuracy, but the upscaling process applied in practice may represent a computational problem with complex geometries. Therefore, more accurate numerical methods and tools are needed to reduce the computational error. Advanced multipoint approximation methods [1]

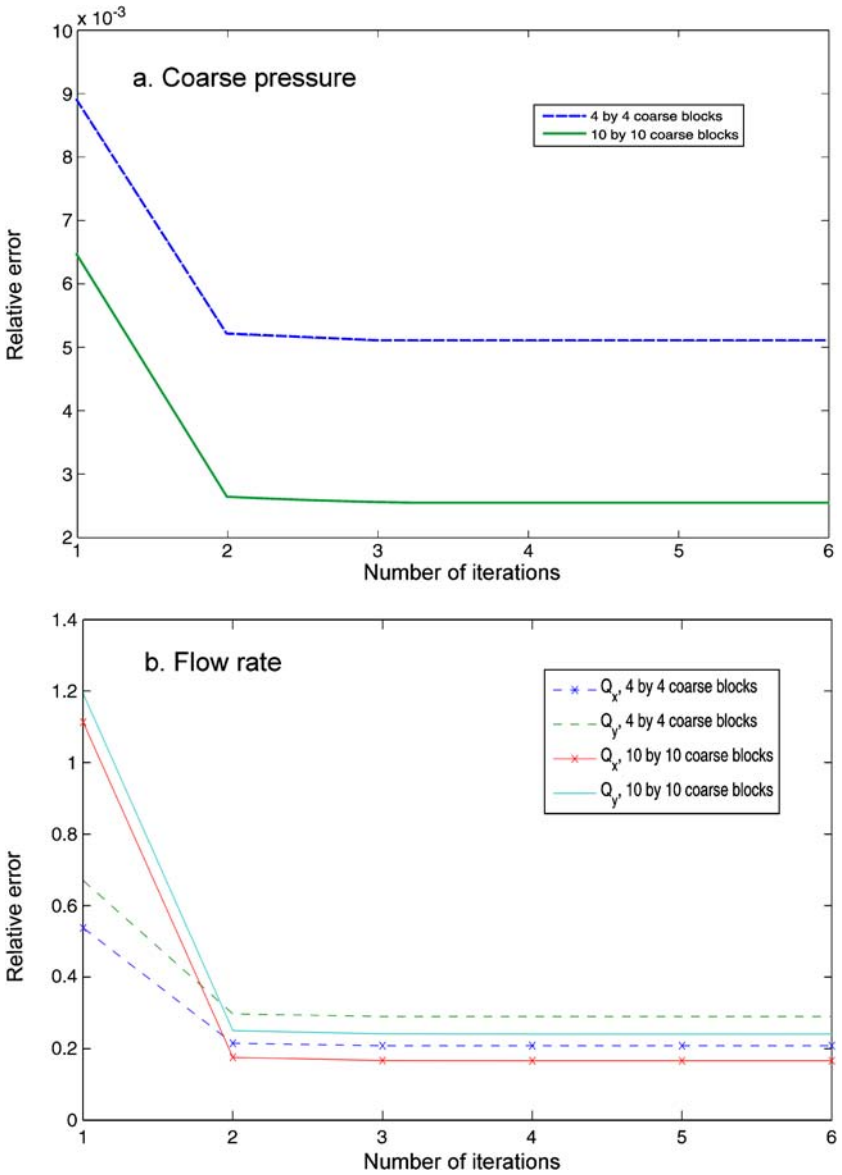

Fig. 14 Accuracy of the upscaled characteristics: **a** coarse grid pressure P_c; **b** flow rates Q in x and y directions. The measure of accuracy is made by comparing the results (X) with the ones obtained at fine scale (X_f): relative error $= \frac{2|X-X_f|}{|X|+|X_f|}$

and nonregular grids may be useful in order to produce reliable results. Further development in multiscale methods may also improve the upscaling methods. But, in many cases, the model error may be the dominating one.

7.2 Results

Our results show that the effect of deformation bands on permeability in the fault damage zone depends on their spatial distribution (clustering), distribution of orientation, and distribution of permeability anomalies or "holes" in the bands. While damage zone flow is overestimated when deformation bands are neglected, quasi 1D models assuming continuous bands with homogeneous permeability oriented perpendicular to the flow direction, as done in the reference model, leads to an underestimation of flow. Figure 16 summarizes the parameters affecting the permeability in the damage zone and illustrates how changes in these parameters can make the effective permeability in the media differ from the permeability calculated analytically in the reference model. More complex and realistic models have been considered through two cases. The first one considers the effect of adding an orientation to the deformation bands (horizontal complexity evolution of the reference model, Fig. 16). The second one takes into account heterogeneous petrophysical properties along the bands. The effect of the different parameters is evaluated by analyzing the relative difference of the

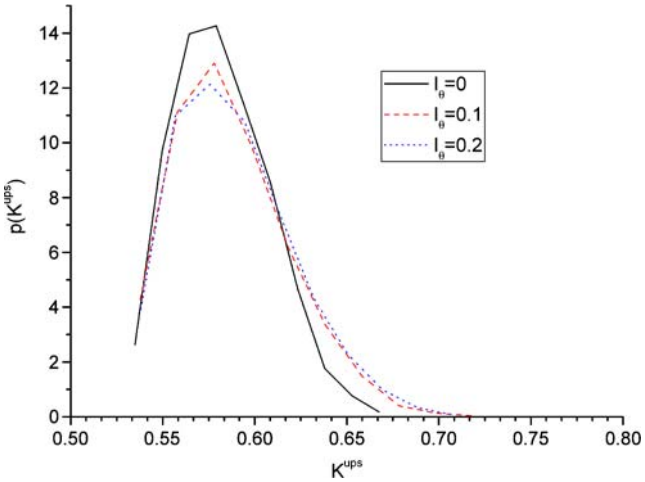

Fig. 15 Probability density of the upscaled permeability. A coarse block of 1 × 1 m is considered. The band density is 10 deformation bands per meter, $K_{DB}/K_{HR} = 0.01$, Dc = 0.8, $\theta = \{\pi/6, -\pi/6\}$; 3,000 realizations of deformation band networks were sampled to estimate the probability density

effective permeability in the more complex models with the permeability defined analytically in the reference model $((K_{eff} - K_{ref})/K_{ref})$.

Adding different orientations to the deformation bands will change the effective permeability of the system. Decreasing the dip angle of the deformation bands will increase the permeability relatively to that of the reference models where the dip angle is 90° (Fig. 8). If the orientations of the dip angles (antithetic or synthetic) are correlated, by imposing a correlation length I_θ, the permeability will be even higher than with a random distribution of orientations (Fig. 7). However, results indicate that the influence of the dip angle value remains higher than having correlated orientations. The discrepancy between the effective permeability and reference permeability can be highly increased if the density of deformation bands and the permeabilities are changed. Increasing the deformation band density (number of deformation bands per meter) leads to a substantial increase in the relative difference between the effective and the reference permeability. Likewise, decreasing the permeability contrast between host rock and deformation bands K_{DB}/K_{HR} causes high relative permeability differences with the reference model. Moreover, strong clustering of the deformation bands will also increase the relative permeability difference regardless of the other parameters. The role of all these parameters (K_{DB}/K_{HR}, density, dip angle, correlation of the dip orientation, and clustering) are interconnected, and the quantification of the effect of one parameter depends on the values of the other parameters; that is why we only give a qualitative and relative influence of all the parameters in Fig. 16.

Another important factor to take into consideration is the heterogeneity of the petrophysical properties. The vertical axis of the graph in Fig. 16 illustrates how variations in permeability along deformation bands can affect the effective permeability of the system and detach it from the reference permeability. The heterogeneity of the deformation band permeability is modeled by introducing "holes" in the deformation bands. Two cases can be pointed out: the first corresponding to a weak clustering of the bands (Dc = 0.8) and the second to a strong clustering (Dc = 0.2). If the clustering is weak, the most important parameter is the degree of fragmentation of the holes. The more fragmented the holes are, the larger the deviation in permeability from the reference model without hole. A secondary parameter to consider is the position of the holes. A uniform position (holes aligned in the model) will favor a larger relative difference. On the contrary, if the clustering is strong, the position of the holes along the bands is the most important parameter, the fragmentation having a minor effect. In damage zones in porous sandstones, the clustering of the deformation bands has been characterized by a correlation dimension close to 0.8. Moreover, observations indicate that the permeability heterogeneity of the bands is more likely to occur like numerous small holes rather than a large singularity. The reference model is, thus, going to give a rather unrealistic estimate of the permeability. If both the orientation, the position of the bands, and the variability in the petrophysical properties of the bands are all taken into consideration (complex model in Fig. 14), then the reference model can give significant errors in permeability estimations.

For example, taking 10 deformation bands per meter (average value observed in normal fault damage zones in sandstones), a permeability contrast of 0.01 and a clustering of 0.8, adding a dip of 60° to the bands and a correlation length I_θ for the dip orientations of 0.1 m, the relative error made on the permeability measurement is equal to $(K_{eff} - K_{ref})/K_{ref} = 17\%$. Increasing the density to 30 deformation bands, which is commonly observed in a damage zone close to the fault core, will lead to a relative error of 29%. These relative errors are quite realistic according to observations made in the field. If the clustering was stronger, then the relative difference with the reference model would be even larger (say, 52% if Dc = 0.2 in our simulations). These results were obtained using local upscaling with diagonal upscaled permeability tensor. However, tests using upscaling methods with a full tensor indicate similar trends. The previous examples

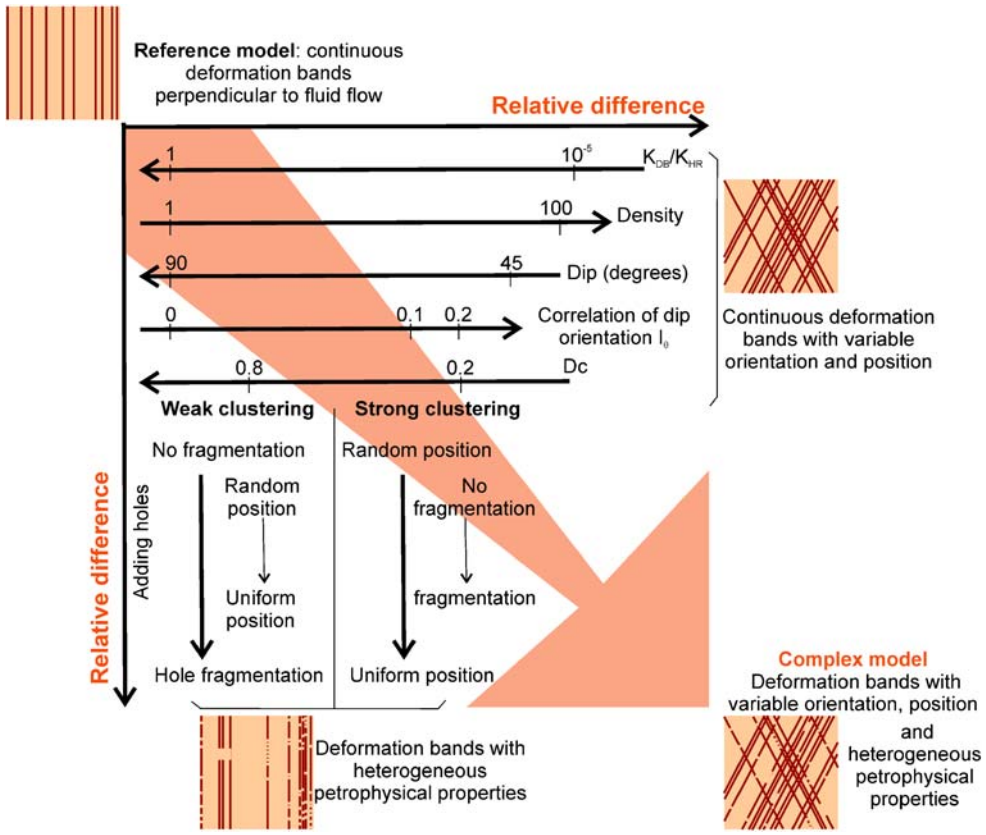

Fig. 16 Summary of the parameters that affect the permeability defined by using the reference model. The reference model corresponds to deformation bands with no orientation (perpendicular to fluid flow) and homogeneous petrophysical properties. Adding an orientation (dip) to the bands will increase the effective flow in the media compared to the reference model. The difference with the permeability calculated for the reference model will be even larger if the permeability contrast between the deformation band and the host rock (K_{DB}/K_{HR}) is small, if the density of deformation bands (number of bands per meter) is large, if the dip angle is low, if the orientations of the dip angle are correlated ($I_\theta \neq 0$) and if the deformation bands are clustered (small Dc). Considering heterogeneous petrophysical properties along the bands by adding "holes" will also increase the relative permeability difference with the reference model. For weak clustering, hole fragmentation is the parameter increasing the most the effective permeability in the system, whereas for strong clustering, the position of the holes along the bands is the most important factor. The complex model corresponds to deformation bands with variable orientations and position in the system and presenting heterogeneous petrophysical properties. This is the model presenting the largest relative difference with the reference model

are given in order to illustrate the underestimation or overestimation of the effective permeability done if geological properties such as variable orientations or heterogeneous petrophysical properties are omitted in the models.

The question how an uncertainty in the coarse block permeability can influence the uncertainty of the productivity of the whole damage zone is still an open question. A simple quasi 1D model is examined in order to get some insights into the problem. The global domain consists in $1 \times M$ coarse blocks ($L_x = 1$ m, L_y=M m, $M = 10$–40). We assume no flow boundary conditions on the borders parallel to the y direction and fixed pressures P_1, P_2 on the borders parallel to x direction. Let the block permeability be $K_i = \alpha K_{\text{ref}} + \sigma_K \xi_i$, where the coefficient α characterizes the relative difference between K_{ref} and the effective permeability ($\alpha = K_{\text{eff}}/K_{\text{ref}}$, $< K > = K_{\text{eff}}$), σ_K the mean deviation of the random variable K, and ξ_i the random variables sampled with standard normal distribution. For the example, the following parameters are taken: the density is 10 deformation bands per meter, $K_{\text{DB}}/K_{\text{HR}} = 0.01$, Dc $= 0.8$, $\theta = \{\pi/6, -\pi/6\}$ and $I_\theta = 0.1$ m. In this case, the numerical calculation give $\alpha = 1.17$, $\sigma_K = 0.03$ darcy. The resulting flux q can be calculated by using Eqs. 2 and 9. We compare an average flux $< q >$ with q_{ref}—flux through the global domain, where each coarse block has a permeability K_{ref}. It is clear that for small σ_K, $< q > / q_{\text{ref}}$ should be approximately equal α. Numerical calculations show that this ratio decreases

slightly with an increase in σ_K. For $1.1 \leq \alpha \leq 1.5$ and $\sigma_K \leq 0.2\ K_{\text{ref}}$, the relative difference $|<q>/q_{\text{ref}} - \alpha|/\alpha$ does not exceed 3.5%.

To estimate the average relative difference $< \|p - p_{\text{ref}}\| > / \|p_{\text{ref}}\|$, the equations for pressure with the original and perturbed permeability derived from correspondent finite-volume approximation are used:

$$\begin{aligned} Ap &= b \\ (A + \delta A)(p + \delta p) &= b\,. \end{aligned}$$

Then, it is possible to estimate the relative pressure perturbation:

$$\left\| A^{-1} \right\| \|\delta A\| \geq \frac{\|\delta p\|}{\|p\|} \geq \left\| \delta A^{-1} \right\|^{-1} \|A\|^{-1}\,. \tag{10}$$

In practice, Eq. 10 gives a very coarse estimation. Numerical calculations show that this relative difference increases linearly with an increase in σ_K. But, for the same values of α and σ_K, it does not exceed 1.6%. However, we should also expect that the relative error increases with increasing coarse block scale and the size of global domain.

From a geological point of view, by considering the clustering of Dc = 0.8 found for the damage zone in sandstones, the petrophysical properties of the bands and their distribution have a relatively larger effect than the orientation variations of the bands. Future works should, thus, focus on better characterizing the petrophysical properties of the faults and more specifically their distribution along the deformation bands.

In addition, improved databases for the most sensitive parameters have to be developed. As noted earlier, the local upscaling procedure seems to be accurate enough to give the trends caused by the variation of different parameters. But for more accurate upscaling required in specific applications or for more complex models, more accurate upscaling tools like the ALG are needed. In this paper, we have discussed the upscaling problem in the global domain and shown the advantage of the ALG upscaling in comparison with the pure local upscaling. However, the numerical results of ALG are presented for only one realization of the bands population, sampled with given probability distribution. Studies based on ALG or other global upscaling methods should be the topic for further research, with a stronger focus on the quantitative parameters describing the models.

Acknowledgements The research was carried out as part of the Fault Facies Project at Centre for Integrated Petroleum Research (CIPR), University of Bergen, Norway. The authors are grateful for financial support from VISTA, a research cooperation between the Norwegian Academy of Science and Letters and StatoilHydro; and from The Research Council of Norway, StatoilHydro and ConocoPhillips.

References

1. Aavatsmark, I.: Multipoint flux approximation methods for quadrilateral grids. In: The 9th International Forum on Reservoir Simulation, Abu Dhabi, 9–13 December 2007
2. Antonellini, M.A., Aydin, A.: Effect of faulting on fluid flow in porous sandstones: petrophysical properties. AAPG Bull. **78**(3), 355–377 (1994)
3. Antonellini, M.A., Aydin, A.: Effect of faulting on fluid flow in porous sandstones: geometry and spatial distribution. AAPG Bull. **79**(5), 642–671 (1995)
4. Beach, A., Welbon, A.I., Brockbank, P.J., McCallum, J.E.: Reservoir damage around faults: outcrop examples from the Suez rift. Pet. Geosci. **5**, 109–116 (1999)
5. Boe, O.: Analysis of the upscaling method based on conservation of dissipation. Transp. Porous Media **17**, 77–86 (1994)
6. Chen, Y., Durlofsky, L.J., Gerritsen, M., Wen, X.H.: A coupled local–global upscaling approach for simulating flow in highly heterogeneous formations. Adv. Water Resour. **26**, 1041–1060 (2003)
7. Chen, Y., Durlofsky, L.J.: Adaptative local–global upscaling for general flow scenarious in heterogeneous formations. Transp. Porous Media **62**, 157–185 (2006)
8. Darcel, C., Bour, O., Davy, P., de Dreuzy, J.R.: Connectivity properties of two-dimensional fracture network with stochastic fractal correlation. Water Resour. Res. **39**(10), 1272 (2003). doi:10.1029/2002WR001628
9. Du Bernard, X., Labaume, P., Darcel, C., Davy, P., Bour, O.: Cataclastic slip band distribution in normal fault damage zones, Nubian sandstones, Suez rift. J. Geophys. **107**(B7), 2141 (2002)
10. Durlofsky, L.J.: Numerical calculation of equivalent grid block permeability tensors for heterogeneous porous media. Water Resour. Res. **27**, 699–708 (1991)
11. Durlofsky, L.J.: Upscaling and griding of fine scale geological models for flow simulation. In: The 8th International Forum on Reservoir Simulation, Iles Borromees, Stresa, Italy, 20–24 June 2005
12. Flodin, E.A., Aydin, A., Durloksky, L.J., Yeten, B.: Representation of fault zone permeability in reservoir flow models. In: SPE 71617. SPE, Houston (2001)
13. Fossen, H., Bale, A.: Deformation bands and their influence on fluid flow. AAPG Bull. **91**(12), 1685–1700 (2007)
14. Fossen, H., Schultz, R.A., Shipton, Z.K., Mair, K.: Deformation bands in sandstone: a review. J. Geol. Soc. **164**, 755–769 (2007)
15. Fowles, J., Burley, S.: Textural and permeability characteristics of faulted, high porosity sandstones. Mar. Pet. Geol. **11**, 608–623 (1994)
16. Grassberger, P., Procaccia, I.: Measuring the strangeness of strange attractors. Physica, D **9**, 189–208 (1983)
17. Hesthammer, J., Johansen, T.E.S., Watts, L.: Spatial relationships within fault damage zones in sandstone. Mar. Pet. Geol. **17**, 873–893 (2000)
18. Holden, L., Nielsen, B.F.: Global upscaling of permeability in heterogeneous reservoirs: the Output Least Square (LOS) method. Transp. Porous Media **40**, 115–143 (2000)

19. Johansen, T.E.S., Fossen, H.: Internal geometry of fault damage zones in interbeded siliciclastic sediments. In: Wibberley, C.A.J., Kurz, W., Imber, J., Holdsworth, R.E., Collettini, C. (eds.) The Internal Structure of Fault Zones: Implications for Mechanical and Fluid-Flow Properties, pp. 35–56. The Geological Society of London, London (2008)
20. Jourde, H., Flodin, E.A., Aydin, A., Durlofsky, L.J., Wen, X.H.: Computing permeability of fault zones in eolian sandstones from outcrop measurements. AAPG Bull. **86**, 1187–1200 (2002)
21. Knott, S.D., Beach, A., Brockbank, P.J., Lawson Brown, J., McCallum, J.E., Welbon, A.I.: Spatial and mechanical controls on normal fault populations. J. Struct. Geol. **18**(2–3), 359–372 (1996)
22. Kumar, A., Farmer, C.L., Jerauld, G.R., Li, D.: Efficient upscaling from cores to simulation models. In: SPE 38744 Annual Technical Conference and Exhibition. SPE, San Antonio (1997)
23. Marchuk, G.I.: Methods of Numerical Mathematics, p. 510. Springer, New York (1982)
24. Odling, N.E., Harris, S.D., Knipe, R.J.: Permeability scaling properties of fault damage zones in siliclastic rocks. J. Struct. Geol. **26**(9), 1727–1747 (2004)
25. Pickup, G.E., Ringrose, P.S., Corbett, P.W.M., Jensen, J.L., Sorbie, K.S.: Geology, geometry and effective flow. Pet. Geosci. **1**(1), 37–42 (1995)
26. Renard, P., de Marsily, G.: Calculating effective permeability: a review. Adv. Water Resour. **20**, 253–278 (1997)
27. Rubinstein, R.Y.: Simulation and the Monte Carlo Method. Wiley, New York (1981)
28. Sanchez-Vila, X., Grirardi, J., Carrera, J.: A synthesis of approaches to upscaling of hydraulic conductivities. Water Resour. Res. **31**(4), 867–882 (1995)
29. Shipton, Z.K., Cowie, P.A.: Damage zone and slip-surface evolution over [mu]m to km scales in high-porosity Navajo sandstone, Utah. J. Struct. Geol. **23**(12), 1825–1844 (2001)
30. Shipton, Z.K., James, J.P., Robeson, K.R., Forster, C.B., Snelgrove, S.: Structural heterogeneity and permeability in faulted eolian sandstones, implications for subsurface modelling of faults. AAPG Bull. **86**, 863–883 (2002)
31. Sternlof, K.R., Karimi-Fard, M., Pollard, D.D., Durlofsky, L.J.: Flow and transport effects of compaction bands in sandstone at scales relevant to aquifer and reservoir management. Water Resour. Res. **42**, W07425 (2006). doi:10.1029/2005WR004664
32. Torabi, A., Fossen, H.: Spatial variation of microstructure and petrophysical properties along deformation bands in reservoir sandstones. AAPG Bull. (2009, in press)
33. Wallace, R.E., Morris, H.T.: Characteristics of faults and shear zones in deep mines. Pure Appl. Geophys. **124**(1, 2), 107–125 (1986)